THE JOURNAL OF BIOLOGICAL CHEMISTRY
Vol. 280, No. 16, Issue of April 22, pp. 16185–16196, 2005

Printed in U.S.A.

The ClpP Double Ring Tetradecameric Protease Exhibits Plastic Ring-Ring Interactions, and the N Termini of Its Subunits Form Flexible Loops That Are Essential for ClpXP and ClpAP Complex Formation*

Received for publication, December 15, 2004, and in revised form, January 21, 2005
Published, JBC Papers in Press, February 8, 2005, DOI 10.1074/jbc.M414124200

Anna Gribun‡§¶, Matthew S. Kimber‖§, Reagan Ching‡ ‡‡, Remco Sprangers‡§§, Klaus M. Fiebig‖, and Walid A. Houry‡¶¶**

From the ‡Department of Biochemistry, University of Toronto, Toronto, Ontario M5S 1A8 and ‖Affinium Pharmaceuticals, Toronto, Ontario M5J 1V6, Canada

ClpP is a conserved serine-protease with two heptameric rings that enclose a large chamber containing the protease active sites. Each ClpP subunit can be divided into a handle region, which mediates ring-ring interactions, and a head domain. ClpP associates with the hexameric ATPases ClpX and ClpA, which can unfold and translocate substrate proteins through the ClpP axial pores into the protease lumen for degradation. We have determined the x-ray structure of *Streptococcus pneumoniae* ClpP(A153P) at 2.5 Å resolution. The structure revealed two novel features of ClpP which are essential for ClpXP and ClpAP functional activities. First, the Ala → Pro mutation disrupts the handle region, resulting in an altered ring-ring dimerization interface, which, in conjunction with biochemical data, demonstrates the unusual plasticity of this region. Second, the structure shows the existence of a flexible N-terminal loop in each ClpP subunit. The loops line the axial pores in the ClpP tetradecamer and then protrude from the protease apical surface. The sequence of the N-terminal loop is highly conserved in ClpP across all kingdoms of life. These loops are essential determinants for complex formation between ClpP and ClpX/ClpA. Mutation of several amino acid residues in this loop or the truncation of the loop impairs ClpXP and ClpAP complex formation and prevents the coupling between ClpX/ClpA and ClpP activities.

Prokaryotic cells respond to stress by activating complex regulatory networks of molecular chaperones, which assist in the proper folding, refolding, or assembly of proteins, and of proteases, which degrade proteins that cannot be refolded (1–3). One such protease is the caseinolytic protease ClpP. ClpP is comprised of two stacked heptameric rings which, in *Escherichia coli*, can form complexes with the ATPase ClpX or ClpA (4–7). ClpX and ClpA are hexameric chaperones that can bind on one or both ends of the ClpP protease. The chaperones bind to target proteins, unfold them, and then thread them into the ClpP proteolytic chamber. These activities require the expenditure of ATP (5, 8–11). In the absence of the ATPase components, ClpP displays limited peptidase activity and can only degrade small peptides of up to six amino acids (12). The functional roles of the ClpXP and ClpAP ATPase-protease complexes include the degradation of misfolded proteins and protein regulation by targeted proteolysis (13–16). ClpXP and ClpAP are highly conserved from bacteria to humans and have served as a model for our understanding of the structure and function of the family of ATP-dependent self-compartmentalizing proteases (17–20). Members of this functional family include the eukaryotic proteasome.

The two heptameric rings of *E. coli* ClpP (*Ec*ClpP)[1] enclose a roughly spherical hollow cavity of about 51 Å in diameter with the 14 proteolytic active sites forming a double ring around the equator of the lumen (21). Structurally, a ClpP monomer can be divided into a head domain, which comprises the bulk of the protein and forms the apical surface of the tetradecamer, and a handle domain consisting of β-strand 9 and helix E, which forms the equatorial wall (21) (Fig. 1). The handle domains of one heptameric ring intercalate with the handle domains of the other heptameric ring to form the tetradecameric ClpP structure. The catalytic triad, Ser^{111}, His^{136}, and Asp^{185}, is located at the junction of the head and handle domains.

In the center of each heptameric ring is a narrow axial pore, lined with the N-terminal most residues of each monomer. Electron microscopy studies have elegantly demonstrated that unfolded polypeptides are translocated into the ClpP proteolytic chamber through this pore (22–24). The molecular details of how the protease interacts with the chaperones and of how

* This work was supported in part by a grant from the Canadian Institutes for Health Research (to W. A. H.). The costs of publication of this article were defrayed in part by the payment of page charges. This article must therefore be hereby marked "*advertisement*" in accordance with 18 U.S.C. Section 1734 solely to indicate this fact.

The atomic coordinates and structure factors (code 1Y7O) have been deposited in the Protein Data Bank, Research Collaboratory for Structural Bioinformatics, Rutgers University, New Brunswick, NJ (http://www.rcsb.org/).

§ These authors contributed equally to this work.

¶ Postdoctoral fellow of the Canadian Institutes for Health Research; recipient of training program grant in protein folding: principles and diseases.

** To whom correspondence may be addressed: Affinium Pharmaceuticals, 100 University Ave, North Tower, 12th floor, Toronto, Ontario M5J 1V6, Canada. E-mail: mkimber@afnm.com.

‡‡ Recipient of a life sciences award from the University of Toronto.

§§ Recipient of a European Molecular Biology Organization postdoctoral fellowship.

¶¶ Canadian Institutes of Health Research new investigator. To whom correspondence may be addressed: 1 King's College Circle, Medical Sciences Bldg., Dept. of Biochemistry, University of Toronto, Toronto, Ontario M5S 1A8, Canada. Tel.: 416-946-7141; Fax: 416-978-8548; E-mail: walid.houry@utoronto.ca.

[1] The abbreviations used are: *Ec*ClpP, *E. coli* ClpP; AMP-PNP, adenosine 5′-(β,γ-imino)triphosphate; ATPγS, adenosine 5′-3-*O*-(thio)triphosphate; E22tr, truncated variant of *Ec*ClpP with the first 7 residues removed; His_6, hexahistidine; HV, His_6 tag followed by a tobacco etch virus cut site; Ni^{2+}-NTA, nickel-nitrilotriacetic acid; *Sp*ClpP, *S. pneumoniae* ClpP; Suc-LY-AMC, *N*-succinyl-Leu-Tyr-7-amido-4-methylcoumarin.

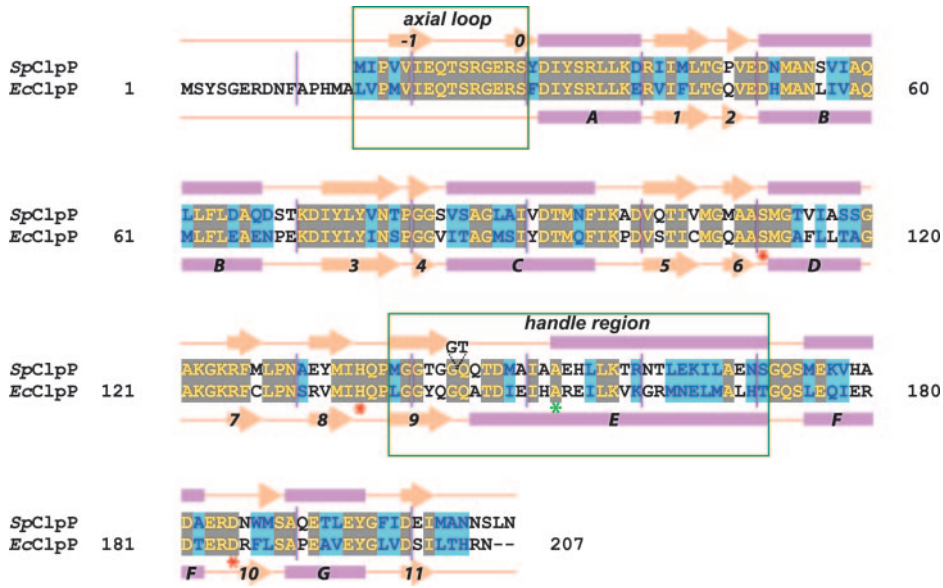

FIG. 1. **Alignment of *S. pneumoniae* and *E. coli* ClpP sequences.** The alignment is based on the Blosum62 matrix used in ClustalW. Identical residues in the two sequences are in *orange*; very similar residues are in *blue*. Residues in the catalytic triad are indicated by *red asterisks*, and Ala[153] is indicated by a *green asterisk*. The axial loop and the handle region are *boxed*. The *numbering* of the helices and strands is the same as that of Wang *et al.* (21).

protein substrates are delivered by the ClpX/ClpA ATPases into the ClpP proteolytic chamber remain poorly understood. Recently, a tripeptide "IGF" motif present in ClpX ("IGL" in ClpA) was found to be essential for the interaction of ClpP with the ATPase. Mutations in this loop destabilize ClpXP complex formation and impair its polypeptide protease activity (25). Joshi *et al.* (26) have demonstrated the presence of functional communication between symmetry-mismatched ClpX and ClpP rings which is mediated, in part, by the IGF loop. Although these interactions are demonstrably necessary for forming a functional complex, it remains unclear as to whether they are sufficient.

Very little is known about the mechanism of release of degraded polypeptides from the ClpP proteolytic chamber. Some investigators have postulated that peptide fragments exit the proteolytic chamber by passive diffusion through the axial pores (21, 24, 27). Other authors have suggested the possible existence of pores, proposed to form at the interface between the two heptameric rings, which may serve as exit holes for peptide fragment release (28–30).

In this study, we show that the truncation of the ClpP handle region β-strand 9 and helix E, which form the main interface between the two heptameric rings of the ClpP tetradecamer, does not lead to a dissociation of the tetradecameric ClpP structure, indicating a high degree of structural plasticity of this region. Furthermore, we were able to solve the x-ray crystal structure of *Streptococcus pneumoniae* ClpP (*Sp*ClpP) with an Ala → Pro mutation (A153P) in helix E of the handle domain (Fig. 1). Although the overall fold of *Sp*ClpP(A153P) is similar to that of *Ec*ClpP (21), the *Sp*ClpP structure shows a different mode of ring-ring interactions because of the A153P mutation, with the last two turns of helix E being unstructured, resulting in the formation of an inactive protease. The structure also shows that the N-terminal most residues of ClpP form flexible loops that protrude above the apical surface. These loops were not observed in the *Ec*ClpP structure (21). We demonstrate that these N-terminal loops are essential for *E. coli* ClpXP/ClpAP complex formation and, in addition to the IGF/IGL loop (25) in ClpX/ClpA, form a second necessary molecular determinant for the interaction between the ATPases and the protease. All biochemical studies described in this paper were carried out using *E. coli* ClpX, ClpA, and ClpP proteins, whereas the structure determined was that of *S. pneumoniae* ClpP(A153P). SwissProt *E. coli* residue numbering is used for both the *E. coli* and *S. pneumoniae* proteases (Fig. 1).

MATERIALS AND METHODS

Subcloning, Mutagenesis, and Protein Purification—pET9aClpP overexpressing untagged wild type *E. coli* ClpP was a gift from Dr. John Flanagan (Brookhaven National Laboratory). pRLM266 overexpressing λO protein was a gift from Dr. Roger McMacken (Johns Hopkins University). pMK951 overexpressing MuA protein was a gift from Dr. George Chaconas (University of Calgary). pET9aClpA(M169T) was a gift from Dr. John Flanagan (Brookhaven National Laboratory). The ClpA protein overexpressed from this plasmid has a M169T mutation that removes an internal translation initiation site (31). In the text, we refer to ClpA(M169T) simply as ClpA. *Sp*ClpP was amplified from *S. pneumoniae* type 14 (ATCC 6314D) genomic DNA and cloned into the NdeI and BamHI sites of a modified pET15b vector, which introduces an N-terminal His_6 tag. The A153P mutation was a fortuitous PCR substitution.

Untagged *E. coli* ClpP, λO, and MuA proteins were purified as described previously (32). All mutated *E. coli* ClpP proteins without prosequence were expressed from p11 vector (a kind gift from Dr. Alexei Savchenko, Clinical Genomic Centre, Toronto) in which gene expression is controlled by a T7 promoter. The vector adds a His_6 tag followed by a tobacco etch virus cut site to the N terminus of the expressed protein (HV tag). Point mutations were introduced using the QuikChange system (Stratagene) according to the manufacturer's protocol. All constructs were verified by DNA sequencing. Tagged proteins were purified according to the manufacturer's protocol (Qiagen). For active ClpPs, the tag was cleaved autocatalytically, whereas for inactive ClpPs, the tag was removed using tobacco etch virus protease. To determine the N-terminal sequence after cleavage, proteins were blotted on polyvinylidene difluoride membrane and then sequenced using an ABI 492 Procise cLC sequencer employing automated Edman degradation chemistry at the Advanced Protein Technology Centre at The Hospital for Sick Children, Toronto. ClpA protein was expressed in BL21(DE3) cells and purified as described previously (33). ClpX was expressed and purified as described by Wojtyra *et al.* (32).

For *Sp*ClpP(A153P), pET15b*Sp*ClpP(A153P) was transformed into BL21(DE3) Gold cells, and a single transformant was cultured in 10 ml of tryptone broth with 50 μg/ml ampicillin at 37 °C until the A_{600} reached 0.8, then transferred into 1 liter of minimal medium supplemented with 50 μg/ml ampicillin and 40 mg L-selenomethionine along with a mix of amino acids calculated to suppress methionine biosynthesis. When an A_{600} of 0.6 was reached, isopropyl-1-thio-β-D-galactopyranoside was added to a final concentration of 0.5 mM, and incubation was continued overnight at 15 °C. Cells were then collected by centrifugation, cell pellets were lysed by sonication, and cell debris was removed by centrifugation. The supernatant containing the soluble protein was applied on a Ni^{2+}-agarose column and purified according to the manufacturer's protocols (Qiagen). The purified protein was concentrated to 40 mg/ml.

Protein concentrations were determined using the Bradford assay (Bio-Rad). All reported concentrations are those for monomers except as indicated.

Crystallization and Structure Determination of SpClpP(A153P)—*Sp*ClpP(A153P) was crystallized by vapor diffusion using 2 μl of 15

TABLE I
Collection and refinement statistics

Data collection statistics		
	λ1(peak)	λ2(remote)
Wavelength (Å)	0.9675	0.9950
Resolution (Å)	30–2.5	30–2.5
No. of observations	407,495	265,388
No. unique	100,999	47,508
Completeness (%)	85.3	89.0
(Last shell)	60.8	71.1
$I/\sigma(I)$	16.6	16.6
(Last shell)	2.6	3.1
R_{symm} (%)[a]	6.4	5.6
(Last shell)	24.1	23.9
Data refinement statistics		
Resolution range (Å)	30–2.5	
R_{cryst}[b]	0.226	
R_{free}[c]	0.269	
R.m.s.d.[d] in		
Bond lengths (Å)	0.008	
Bond angles (°)	1.4	
Dihedral angles (°)	22	
Improper angles (°)	0.99	

[a] $R_{symm} = \Sigma_{hkl} \Sigma_i |I_i - \langle I \rangle| / \Sigma_{hkl} \Sigma_i \langle I \rangle$, where I_i is the ith measurement of the reflection intensity I, and $\langle I \rangle$ is the weighted mean of all measurements of I.

[b] $R_{cryst} = \Sigma_{hkl} |F_{obs} - F_{calc}| / \Sigma_{hkl} F_{obs}$, where F_{obs} and F_{calc} are the observed and the calculated amplitudes, respectively, and the summation is over the 90% of reflections used for model refinement.

[c] R_{free} is the same as R_{cryst} except summed only over the 10% of randomly selected reflections not used for model refinement.

[d] R.m.s.d., root mean square deviation.

mg/ml protein plus 2 μl of well solution (containing 29% polyethylene glycol 400, 0.2 M calcium acetate, and 0.1 M sodium cacodylate at pH 7.0) in a hanging drop configuration. Crystals grew to 250 μm and were flash frozen in a liquid nitrogen stream after a brief soak in two parts of the above well solution diluted with one part of polyethylene glycol 400. Data were collected at the Advanced Photon Source beamline ComCAT, Illinois. Two passes of data were collected at the selenium anomalous peak and at the low energy remote wavelength for the purposes of phasing. Selenomethionyl crystals of *Sp*ClpP(A153P) diffracted to a resolution of 2.5 Å and were found to belong to the trigonal space group $P3_221$ with cell dimensions $a = b = 104.335$ Å, $c = 244.243$ Å. Data were processed using the program Denzo and scaled using Scalepack (34).

The intensity data were converted to structure factors, and a random subset of 10% of the reflections was selected and removed from the refinement for cross-validation purposes. Anomalous substructure searching, refinement, experimental phasing, and density modification were performed using standard procedures in CNX (35). Automated heavy atom searching found 84 selenium sites; after refinement, this yielded useful phases with an overall 0.279 figure of merit and phasing power of 1.26. This yielded a partial model that subsequently was fully built using the program Turbo-Frodo (36). Data collection, processing, and phasing statistics are given in Table I.

Refinement was conducted in CNX against the remote data using a maximum likelihood function that includes the experimental phases as part of the target. Successive rounds of model rebuilding and adding solvent molecules followed by positional and restrained individual B refinements produced the current model with R_{cryst} of 0.226 (R_{free} = 0.269). Structure refinement statistics are given in Table I. The final model contains 177 water molecules and is missing the following residues: chain A, 24–29, 140–151, and 207–209; chain B, 25–27, 140–150, and 208–209; chain C, 24–28, 140–151, and 209; chain D, 27, 140–151, and 208–209; chain E, 23–28, 140–151, and 208–209; chain F, 1, 21–28, 140–151, and 209; chain G, 1, 24–27, 140–150, and 209. All structure figures were prepared using PyMol (pymol.sourceforge.net/).

Size Exclusion Chromatography—Gel filtration was performed using a calibrated Superdex 200 HR 10/30 column (Amersham Biosciences) attached to an AKTA fast protein liquid chromatography system (Amersham Biosciences). The column was equilibrated with buffer A (25 mM Tris-HCl, pH 7.5, 200 mM NaCl, 10% glycerol, and 1 mM dithiothreitol). Molecular mass standards (Sigma) used were: thyroglobulin (669 kDa), apoferritin (443 kDa), β-amylase (200 kDa), alcohol dehydrogenase (150 kDa), bovine serum albumin (66 kDa), carbonic anhydrase (21 kDa), and cytochrome *c* (12.4 kDa). All experiments were performed at 4 °C, and absorbance was monitored at 280 nm.

Circular Dichroism Measurements—CD spectra were obtained using a Jasco J-810 spectropolarimeter equipped with a Peltier temperature control device. The average of three spectra is reported. Each spectrum was collected by averaging the signal at every 0.1 nm for 4 s. The protein concentration was 20 μM in buffer B (25 mM Tris-HCl, pH 8, 150 mM NaCl, and 1 mM dithiothreitol). A 1-mm path length cuvette was used, and the temperature was set at 22 °C.

Peptidase Assays—Peptidase activity at 37 °C of wild type ClpP and of its different mutants was quantified by measuring the rate of cleavage of the fluorogenic peptide *N*-succinyl-Leu-Tyr-7-amido-4-methylcoumarin (37) (Suc-LY-AMC) purchased from Sigma. 0.2 μM ClpP was dissolved in buffer C (50 mM Tris-HCl, pH 7.5, 200 mM KCl, and 1 mM dithiothreitol) and incubated for 3 min. 0.5 mM Suc-LY-AMC was then added, and the fluorescence increase caused by the formation of free AMC was monitored for 10 min on a Fluorolog 3-222 spectrofluorometer (Jobin Yvon) using an excitation wavelength of 360 nm and an emission wavelength of 440 nm. Degradation assays of model substrates by ClpXP and ClpAP were carried out as described previously (32). ClpAP degradation assays were carried out in buffer D (25 mM HEPES, pH 7.5, 150 mM NaCl, 10 mM $MgCl_2$, and 10% glycerol).

Light Scattering Assays—The assembly of ClpXP and ClpAP complexes was monitored by changes in light scattering of protein solution as described by Singh *et al.* (38). Measurements were performed at room temperature using a Fluorolog 3-222 spectrofluorometer with the excitation and emission wavelengths set at 360 nm and slits set to 4 nm. All solutions were filtered through 0.2-μm syringe filters (Gelman Laboratories). Typically, 1 μM ClpX or ClpA was added to buffer in the presence or absence of ATPγS followed by the addition of 1.2 μM ClpP. Proteins were incubated for 5 min, and, subsequently the intensity of 90° scattered light was averaged over 50 s. The signal intensity of buffer was subtracted from all experiments.

Binding Assays—For pull-down assays, each reaction contained 1 μM HV-ClpX (wild type), 1.8 μM ClpP (wild-type and mutants), and 2 mM AMP-PNP (Sigma) in a total volume of 50 μl, whereas control reactions contained only 1 μM HV-ClpX and 2 mM AMP-PNP. After equilibration with Ni^{2+}-NTA resin at 30 °C, the mixture was applied onto Micro Bio-Spin chromatography columns (Bio-Rad), and unbound proteins were washed three times with 200 μl of buffer E (2.5 mM HEPES, 2.5 mM $MgCl_2$, 2.5 mM KCl, 100 mM imidazole, 0.015% Tween 20, 5% glycerol, and 2 mM ATP). Bound proteins were eluted using 50 μl of buffer F (2.5 mM HEPES, 2.5 mM $MgCl_2$, 2.5 mM KCl, 250 mM imidazole, 0.015% Tween 20, 5% glycerol, and 2 mM ATP), separated on 12% SDS-PAGE, and silver stained.

The binding of ClpX to ClpP(E28W) was assayed by monitoring the change in tryptophan fluorescence of ClpP(E28W) because wild type ClpX and ClpP have no tryptophans. 2.1 μM ClpP(E28W) was incubated in buffer A with 1 mM ATP at 37 °C. After 3 min of incubation, ClpX was added at different concentrations, and fluorescence emission scans were obtained using an excitation wavelength of 295 nm. Each experiment was carried out in triplicate. Background intensities, without ClpP(E28W), were subtracted from all experimental data points, and scans were corrected for ClpP concentration. A saturation curve for ClpX-ClpP(E28W) complex formation was obtained, and K_d values were calculated using the Scatchard equation assuming, for simplicity, n identical and independent weak binding sites in $ClpP(E28W)_{14}$ for $ClpX_6$.

$$r/[\text{free } ClpX_6] = n/K_d - r/K_d \quad \text{(Eq. 1)}$$

where

$$r = [\text{bound } ClpX_6]/[\text{total } ClpP(E28W)_{14}] \quad \text{(Eq. 2)}$$

RESULTS

Disruption of the Handle Domain Does Not Prevent Ring-Ring Interactions in the ClpP Tetradecamer—To study the properties of the handle region and to determine its contribution to ring-ring interactions, we expressed, purified, and characterized three point mutants and three variants of *Ec*ClpP with deletions in the handle region (Fig. 1): ClpP(A153P), ClpP(E183A), ClpP(R184G), ClpP(Δ139–155), ClpP(Δ142–152), and ClpP(Δ145–149). The A153P mutation was chosen because we were able to solve the structure of that mutant from

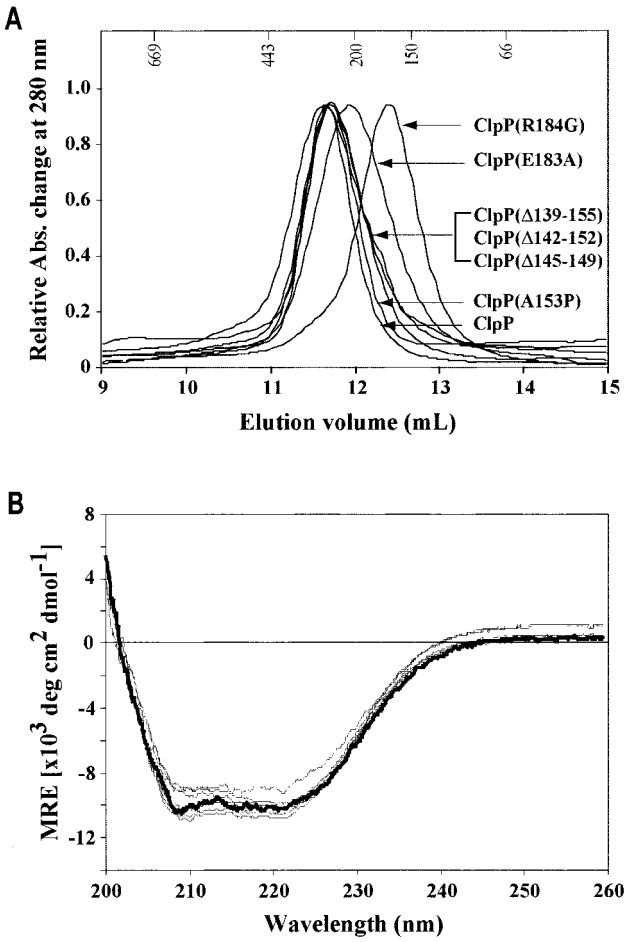

FIG. 2. **Residues in the handle region are not essential for the formation of ClpP double ring structure.** *A*, the oligomeric state of wild type ClpP and of the different indicated mutants was determined using size exclusion chromatography on a calibrated Superdex 200 HR 10/30 column equilibrated with buffer A at 4 °C. Wild type ClpP and the different mutants eluted as double rings with the exception of ClpP(R184G), which eluted as a single ring, and ClpP(E183A), which eluted as a mixture of single and double rings. The positions of the molecular mass standards, in kDa, are indicated on the *upper x axis*. *B*, far-ultraviolet CD spectra at 22 °C of wild type ClpP (*dark line*) and the different mutants listed in *A* (*thin lines*) equilibrated in buffer B. The CD signal is expressed as the mean residue ellipticity (*MRE*).

S. pneumoniae (see below). All proteins were expressed with a polyhistidine tag followed by a tobacco etch virus cut site (HV tag) fused to the N-terminal Met^{14} residue of ClpP lacking the pro-sequence (HV-ClpP) for rapid purification on Ni^{2+}-NTA-agarose columns (39).

All of these mutants were inactive as judged by their inability to cleave the HV tag autoproteolytically as indicated by SDS-PAGE analysis (data not shown). They were also unable to cleave the fluorogenic Suc-LY-AMC peptide (data not shown), which is a known *Ec*ClpP model peptide substrate (37). Moreover, in the presence of ClpX, none of the mutants mediated the degradation of model protein substrates such as GFP-SsrA, λO, and MuA (data not shown). We propose that this functional impairment is because of the proximity of the mutations/truncations to the active site of ClpP as suggested by the structure described below.

Surprisingly, neither the truncations nor the A153P mutation in helix E affected the oligomeric state of $EcClpP_{14}$. As shown by size exclusion chromatography in Fig. 2*A*, the truncation of β-strand 9 and/or helix E or the introduction of a proline in that helix (A153P) did not affect the elution profile of these mutants compared with wild type ClpP, indicating that these mutants eluted as double rings. However, the mutation of charged residues located at the C terminus of helix F (Fig. 1) causes a shift in the elution profile of ClpP oligomers toward a lower apparent molecular mass: ClpP(R184G) eluted as a single ring, whereas ClpP(E183A) eluted as a mixture of single and double rings. These results were verified further by analytical ultracentrifugation (data not shown). CD spectra of the discussed mutants indicate that the mutants have similar overall secondary structure composition compared with that of wild type protein (Fig. 2*B*). These observations indicate ClpP is able to employ alternative modes of ring-ring interactions which can compensate for mutational disruptions in the handle region and still achieve ring dimerization, albeit in a catalytically compromised state.

Overall Structure of SpClpP(A153P)—We determined the crystal structure of the *Sp*ClpP(A153P) mutant to a resolution of 2.5 Å by a combination of molecular replacement and single anomalous scattering (for data collection, phasing, and structure refinement statistics, see Table I).

As shown in Fig. 1, there is a high degree of sequence identity between the *E. coli* and *S. pneumoniae* proteins; hence, it is not surprising that the structure of *Sp*ClpP(A153P) reported here closely resembles the previously reported *Ec*ClpP structure (PDB 1TYF) (21). Using the "magic fit" algorithm of the Spdbv molecular viewing and manipulation program (40), 4,476 atoms from the two monomers can be overlaid with a root mean square deviation of 1.37 Å; this reflects a close overall similarity, especially in the head domain (Fig. 3, *A* and *B*). However, there are two regions in the *Sp*ClpP(A153P) structure which differ substantially from the *Ec*ClpP structure: the handle domain and the N-terminal loops. These differences have important functional implications as discussed below.

The SpClpP(A153P) Structure Displays a Novel Mode of Ring-Ring Contacts—A key difference between the *Sp*ClpP(A153P) and *Ec*ClpP structures lies in the region immediately N-terminal to the A153P mutation because residues 140–151 in the *Sp*ClpP(A153P) structure are disordered in all monomers (Fig. 3*B*). Careful examination of both experimental and difference maps phased with a combination of model and experimental phases revealed no plausible density for these 14–15 residues (*Sp*ClpP has a 2-residue insertion in this region relative to *Ec*ClpP (Fig. 1), and residue 139 is disordered in a subset of the chains). Instead, the location of the last residues flanking the missing region that were visible in the electron density map localize to the luminal interior of *Sp*ClpP(A153P). This implies that the disordered residues are most likely present as unstructured loops within the protease lumen. In the *Ec*ClpP structure, the equivalent residues form the handle domain, a strand-turn-helix motif that mediates almost all of the interactions between the two heptameric rings by forming a two-stranded β-sheet with the strands contributed from distinct monomers in each ring and by packing helix E in one subunit against the same helix in another subunit on the opposite ring. In the *Sp*ClpP(A153P) structure, the last two turns of this helix are disordered, along with most of the residues of β-strand 9, and hence the two rings are associated through a radically different mechanism than that observed in the *Ec*ClpP structure. None of the interactions between rings seen in the *Ec*ClpP structure was observed in the *Sp*ClpP(A153P) structure. This has important consequences for the relative positioning of the two heptameric rings.

In each heptameric ring, the structure, orientation, and packing of the head domains of *Sp*ClpP(A153P) and *Ec*ClpP are nearly identical. Using the lower ring as the point of reference, the upper ring in *Sp*ClpP(A153P) is shifted down with respect to the position of the upper ring in *Ec*ClpP (Fig. 3, *C* and *D*),

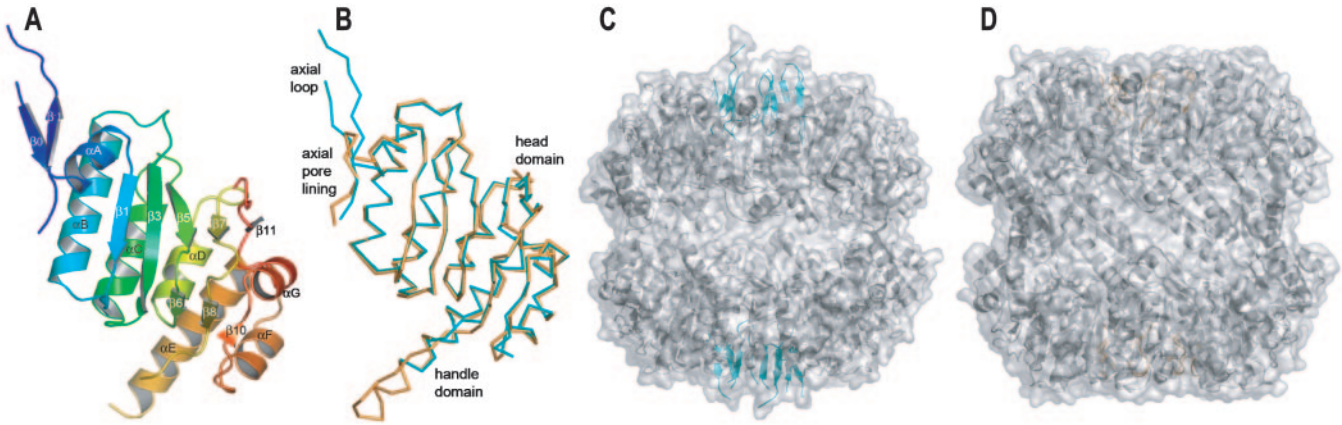

FIG. 3. **Overall structure of the *Sp*ClpP(A153P) protein.** *A*, *ribbon* representation of *Sp*ClpP(A153P) monomer. *B*, overlay of the monomer of *Ec*ClpP (PDB code 1TYF) drawn in *orange* on *Sp*ClpP(A153P) drawn in *cyan*. *C*, side view of the *Sp*ClpP(A153P) tetradecamer showing backbone and transparent surfaces. The N-terminal axial loops are shown as *blue ribbons*. *D*, same as *C* but for *Ec*ClpP. The *Ec*ClpP tetradecamer is longer, in the axial direction, than *Sp*ClpP(A153P). The N-terminal axial loops are shown in *orange*.

and this causes helix E in *Sp*ClpP(A153P) to be shifted almost two full turns along the same axis. Viewed from above, the upper ring of the *Sp*ClpP(A153P) tetradecamer is rotated ~10° counterclockwise and translated ~6 Å closer to the opposite ring. This makes the overall *Sp*ClpP(A153P) oligomer and the internal chamber proportionately smaller compared with *Ec*ClpP. One consequence of this rearrangement is a large loss of ring-ring binding surface. The handle domain of a given subunit in *Ec*ClpP buries in total 775 Å^2 solely by interacting with the handle domain of the subunit in the opposite ring. However, for *Sp*ClpP(A153P), each handle domain buries only 270 Å^2 in interactions with the monomer directly opposite on the interacting ring, and 96 Å^2 by interacting with a neighboring subunit from the partner ring (Fig. 4, *A* and *B*). The imperfect packing of the two rings in the *Sp*ClpP(A153P) structure results in a set of irregular pores formed around the equator of the complex with dimensions of ~5 Å × 10 Å (Fig. 4*B*). Residues contributing to the lining of the pore include Arg^{160}, His^{179}, and Glu^{183} of one monomer, Ile^{151}, Ala^{152}, and Glu^{154} of a second monomer from the same ring, and Arg^{184}, Asp^{185}, Asn^{186}, and Trp^{187} of a third monomer from the opposite ring.

The A153P mutation in *Sp*ClpP also affects the structural integrity of the active site. In the *Ec*ClpP structure, Ser^{111}, His^{136}, and Asp^{185} approach one another to form a slightly distorted catalytic triad (Fig. 4*C*), which is nevertheless able to react with inhibitors such as benzamidine (21). For *Sp*ClpP(A153P), the underlying secondary structural elements necessary for the proper orientation of the residues of the catalytic triad have been displaced: Asp^{185} is shifted ~2 Å away from the rest of the triad, and His^{136}, as a consequence of the repacking of residues at the end of β-strand 9, is flipped into an orientation where it can no longer interact with either of the other 2 residues (Fig. 4*D*). Furthermore, the disordering of β-strand 9, which is part of the handle domain and is believed to act as a guide for substrate binding (21), would result in a site that cannot properly bind substrates. In summary, these structural observations strongly suggest that *Sp*ClpP(A153P) is a proteolytically inactive tetradecamer, which is in agreement with our experimental results with the *Ec*ClpP(A153P) ortholog.

N-terminal Axial Loops in the SpClpP(A153P) Structure Show Flexibility and Structural Heterogeneity—In the *Sp*ClpP(A153P) crystal, the N-terminal most residues of a monomer in one ring (Met^{16}–Ser^{30}) form a loop that is anchored in the axial pore with a protruding region that is partially stabilized by packing interactions with the N-terminal end of a second ring of the crystal lattice. The quality of density in this region varies from loop to loop, causing anywhere from 2 to 8 residues in the center of the loop to be untraceable (Fig. 5*A*). The N-terminal loop can be divided into two parts. The first part, termed the "axial pore lining," comprises hydrophobic residues Met^{16}–Ile^{21}, which line the axial pore and are stabilized by interactions with the head domain (Fig. 5, *B* and *C*). Met^{16} resides inside the protease chamber with its Cα atom about 20 Å from the apical surface. The second part, termed the "axial protrusion," comprises residues Glu^{22}–Ser^{30}. These residues are predominantly charged or hydrophilic and form an extended loop protruding as much as 15 Å beyond the apical surface (Fig. 3*C* and Fig. 5, *B* and *C*). Typically, residues Glu^{22}–Ser^{25} trace away from the ClpP apical surface, whereas residues Glu^{28}–Ser^{30} trace back toward the head domain. Tyr^{31} and Asp^{32} connect the loop to helix A. The conformation of the loop differs substantially from one monomer to the other (Fig. 5*D*).

In contrast, the N terminus, as modeled in the *Ec*ClpP structure, does not protrude beyond the apical surface of the head domain (21) (Figs. 3*D* and 5*E*). Residues Ser^{30} and Phe^{31} in *Ec*ClpP form a β-turn, and this causes the residues that comprise the axial protrusion in the *Sp*ClpP(A153P) structure to form the axial pore lining in *Ec*ClpP (Fig. 5*E*). As a consequence, the large basic residues Arg^{26} and Arg^{29} point into the axial pore (Fig. 5*E*), making the pore entrance narrow (~10 Å) and highly basic (net charge of +14). In the *Sp*ClpP(A153P) structure, in contrast, the side chains of the small hydrophobic residues Val^{19} and Ile^{21} point into the pore (Fig. 5*C*), resulting in a greatly increased pore diameter of ~17 Å in this region (Fig. 5*B*). A hydrophobic rather than basic pore also provides an environment more conducive to keeping unfolded proteins in an extended conformation. Wang *et al.* (21) had suggested that there may be significant uncertainty in the tracing of the N-terminal loop in their *Ec*ClpP model as a result of poor electron density in that region. We believe that the *Sp*ClpP(A153P) structure provides a better model for this region because of the clearer electron density in addition to other experimental data presented below.

ClpP N-terminal Loops Modulate Peptide Diffusion through the Axial Pores—Multiple sequence alignment of more than 100 ClpP sequences derived from different prokaryotic and eukaryotic genomes shows a very high degree of sequence conservation in the N terminus (Fig. 6*A*). This likely indicates that this region forms a well conserved, functionally important structure. One possible role for the N-terminal axial loops is to mediate the interaction between ClpP and its ATPases, ClpX

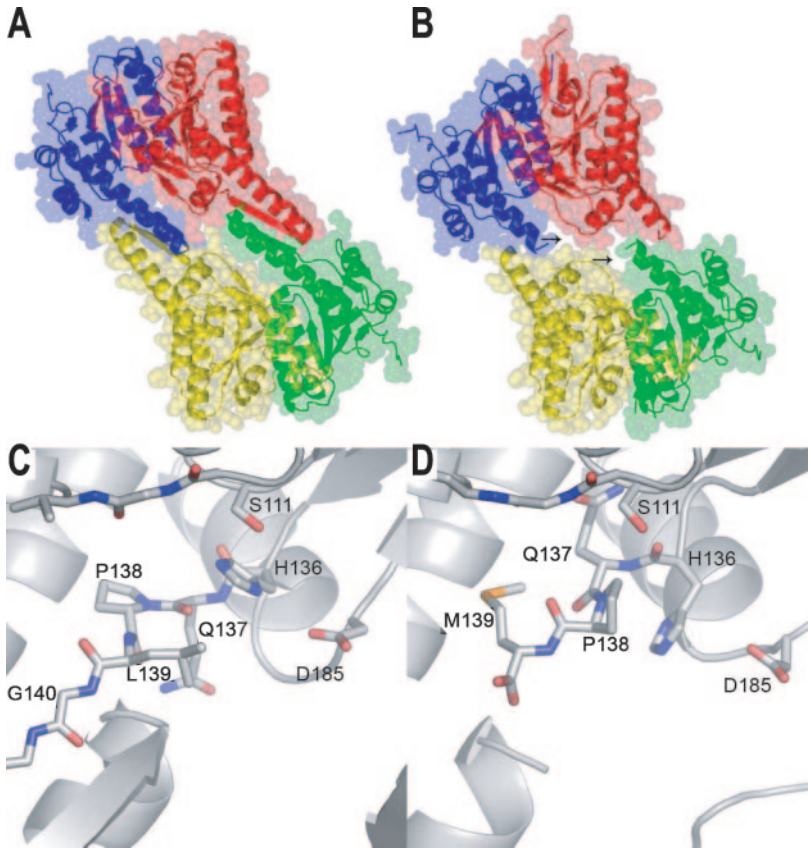

FIG. 4. **Structural and functional consequences of the *Sp*ClpP A153P mutation.** *A*, *color* representation of four monomers in the *Ec*ClpP tetradecamer overlaid with a transparent set of van der Waal spheres. Two monomers (in *red* and *blue*) are from one heptameric ring, and the other two monomers (in *yellow* and *green*) are from the opposite heptameric ring. The molecule is oriented so that the 7-fold axis is *vertical*. Note that the two rings fit snugly, with extensive interactions between the handle domain of the respective rings. *B*, same as *A* but for *Sp*ClpP(A153P). The opening of gaps between the rings, indicated by *arrows*, can be seen. The two rings now interact along a relatively flat surface rather than by interdigitation. None of the interactions that mediate interring packing in the *Ec*ClpP structure is observed in the *Sp*ClpP(A153P) structure. *C*, *ribbon and stick diagram* of the *Ec*ClpP active site. Ser^{111}, His^{136}, and Asp^{185}, which are believed to form a catalytic triad, are subtly misaligned, but, given that the crystals retain a reactivity to the protease inhibitor benzamidine (21), the triad would seem to be properly formed at least part of the time. The extended β-strand 9 of the handle domain (residues 139–144) is thought to function as a guiding strand that helps to orient peptides in the catalytic site. *D*, the *Sp*ClpP(A153P) active site. The structural rearrangements associated with the partial disordering of the handle domain result in the displacement of several key components of the catalytic site. His^{136} is flipped into a conformation where it is no longer close to Ser^{111}, Asp^{185} is moved away from His^{136} via main chain motions, and β-strand 9 is disordered.

and ClpA. To investigate this possibility, amino acid substitutions were introduced by site-directed mutagenesis at six highly conserved N-terminal positions (P18G, V20H, E22G, R26G, E28G, R29G), and a truncated variant of *Ec*ClpP was made with the first 7 residues removed (E22tr) compared with processed wild type *Ec*ClpP. In the cell lysate, with the exception of the P18G mutant, which remained uncleaved, overproduced HV-ClpP mutants, which have the HV tag fused directly to the mature *Ec*ClpP sequence starting at Met^{14}, separated on SDS-polyacrylamide gels as two bands with molecular masses of 21 and 23 kDa, suggesting that both processed and unprocessed forms of the protease are present. These forms were also seen when purified proteins were eluted from the Ni^{2+}-NTA-agarose. However, after overnight dialysis at room temperature only the 21 kDa band was detectable on silver-stained gels, indicating that the protein was fully processed. The N-terminal sequence of one of the point mutants (R29G) was determined by Edman degradation to be identical to that of processed wild type ClpP (Ala^{15}-Leu^{16}-Val^{17}-Pro^{18}-Met^{20}), and the N terminus of processed ClpP(E22tr) was found to be as expected (Glu^{22}-Gln^{23}-Thr^{24}-Ser^{25}-Arg^{26}). ClpP(P18G) was not processed at all and was not studied further, whereas ClpP(V20H) was not processed to completion (Fig. 6*B*).

Size exclusion chromatography of ClpP N-terminal mutants showed that these mutants had mobility similar to that of wild type ClpP (Fig. 6*B*), implying the formation of double rings. The mobility of ClpP(R184G) single ring is shown as a reference (Fig. 6*B*). Furthermore, based on CD spectra (Fig. 6*C*), all of the mutants had an overall secondary structure composition similar to that of the wild type protease. The peptidase activity of the ClpP N-terminal mutants was measured using Suc-LY-AMC fluorogenic peptide as substrate (37). As expected, the initial peptide cleavage rates obtained for ClpP N-terminal point mutants are similar to those of wild type ClpP (Fig. 6*D*). However, ClpP(E22tr) exhibited an initial catalytic rate twice that of wild type ClpP (Fig. 6*D*). These results indicate that mutations at the N-terminal loop of ClpP do not inhibit the peptidase activity of the protein. However, intriguingly, increasing the size of the axial pores by deleting some of these N-terminal residues enhances the rate of degradation of the model peptide, possibly by allowing easier access into the protease active core.

Mutations in the N-terminal Loop of ClpP Affect ClpXP and ClpAP Degradative Activities—ClpP has to interact with the ATPase ClpX or ClpA to degrade larger polypeptides. When in complex with the protease, the ATPases can bind, unfold, and then translocate target substrates into the ClpP catalytic core. Hence, to determine whether the N-terminal loop of ClpP is required for the interaction of the protease with ClpX and ClpA, degradation assays of specific ClpXP model substrates

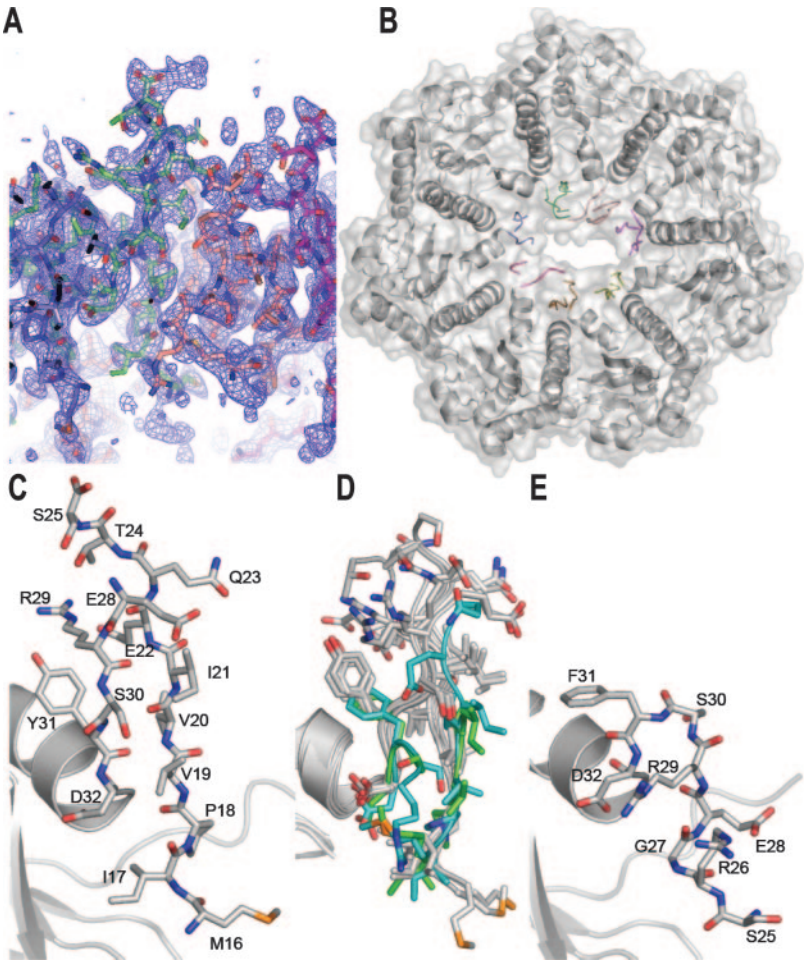

FIG. 5. **Structure of the N-terminal axial loops.** *A*, σA-weighted $2F_o - F_c$ electron density at 1σ in the N-terminal loop region of chain D. Carbon atoms are *colored* differently for different chains. *B*, top view of the *Sp*ClpP(A153P) tetradecamer showing backbone and transparent surfaces looking down the 7-fold axis. The N-terminal loop of each monomer is *colored* differently, and the rest of the molecule is shown in *white*. In contrast to the rest of the ring, the axial pore is quite asymmetric. *C*, detail of a representative N-terminal axial loop looking across the pore. Residues 16–32 of chain D are drawn in *stick representation*, whereas the rest of the structure is drawn in *cartoon representation*. The 7-fold symmetry axis is oriented *vertically*. Residues are labeled in accordance with the SwissProt *Ec*ClpP numbering. *D*, overlay of the N-terminal loops of seven monomers from one ring in the asymmetric unit of the *Sp*ClpP(A153P) crystal. Five monomers that resemble the conformer in *B* are shown in *white*; the two monomers shown in *green* and *cyan* deviate markedly from this consensus, being partially displaced into the pore. *E*, structure of residues 25–32 in *Ec*ClpP (21). Residues 31–32 form a β-turn, whereas residues N-terminal to Ser^{25} are not resolved.

(GFP-SsrA, MuA, and λO) were carried out in the presence of ClpP mutants, ClpX, ATP, and an ATP-regenerating system. With the exception of ClpP(E28G) and ClpP(E28W), none of the other ClpP N-terminal mutants was able to degrade these model substrates (Fig. 7, *A* and *B*). Degradation assays of GFP-SsrA using the inactive ClpP(A153P) are shown as a reference (Fig. 7, *A* and *C*). In the presence of ClpX, ClpP(E28G) and ClpP(E28W) degraded GFP-SsrA at initial rates that were 66 and 50% that of wild type protease (Fig. 7*A*), respectively. They were also able to degrade λO and MuA, albeit at slower rates compared with wild type ClpP (Fig. 7*B*). Similar results were obtained for the degradation of GFP-SsrA by ClpAP (Fig. 7*C*). With the exception of ClpP(E28G) and ClpP(E28W), none of the other ClpP N-terminal mutants was able to degrade GFP-SsrA in the presence of ClpA.

The fact that truncating the N terminus of ClpP (ClpP(E22tr)) or mutating 1 of 4 highly conserved residues at the N terminus of the protease (Val^{20}, Glu^{22}, Arg^{26}, and Arg^{29}) renders ClpP ineffective in degrading model proteins, but not small peptides (Fig. 6*D*), strongly suggests that the ClpP N terminus is required for the proper formation of active ClpXP and ClpAP complexes.

Direct Evidence for the Interaction of the ClpP N-terminal Loop with ClpX and ClpA—To obtain more direct evidence for the role of the ClpP N terminus in mediating the interaction between the protease and ClpX, pull-down experiments were carried out of untagged ClpP mutants by HV-ClpX in the presence of 2 mM AMP-PNP using Ni^{2+}-NTA beads (Fig. 8*A*). Control pull-down experiments of the different ClpP mutants were carried out in the absence of HV-ClpX. Only wild type ClpP, ClpP(E28W), and ClpP(E28G) were pulled down with HV-ClpX. None of the other N-terminal ClpP mutants showed significant binding to HV-ClpX in this assay.

Because ClpX and ClpP have no tryptophan residues, this enabled us to use changes in tryptophan fluorescence of ClpP(E28W) to monitor directly the interaction between ClpP and ClpX in the presence of ATP. The tryptophan fluorescence of ClpP(E28W), using an excitation wavelength of 295 nm, was enhanced upon addition of ClpX, and the emission maximum was shifted from 350 nm to slightly shorter wavelengths (Fig. 8*B*). This is consistent with the tryptophan being solvent-exposed in ClpP(E28W) and becoming buried in a hydrophobic environment upon binding of ClpX (41). A plot of ClpX concentration *versus* relative fluorescence change at 350 nm gave a typical binding curve (Fig. 8*C*). Analysis of the data using a Scatchard plot (Fig. 8*C*, *inset*) assuming, for simplicity, *n* identical and independent weak binding sites for $ClpX_6$ on $ClpP(E28W)_{14}$ (see "Materials and Methods") gave a dissociation constant (K_d) of 210 nM and $n = 1.5$, indicating that saturation is probably reached when two $ClpX_6$ bind to $ClpP(E28W)_{14}$. Because ClpP(E28W) seems to bind ClpX less strongly than wild type ClpP (Fig. 8*A*) and, in the presence of ClpX/ClpA, degrades substrates at a slower rate than that of wild type protease (Fig. 7), we predict that K_d for the binding between wild type ClpP and ClpX might even be lower. Our values are in general agreement with the previously estimated K_d value of 90 nM for the binding of $ClpP_{14}$ to $ClpX_6$ obtained based on ATP turnover measurements (26). Such fluorescence-based experiments could not be carried out with ClpA because, unlike ClpX, this chaperone includes multiple tryptophan residues in its sequence.

Light scattering experiments further corroborated the above

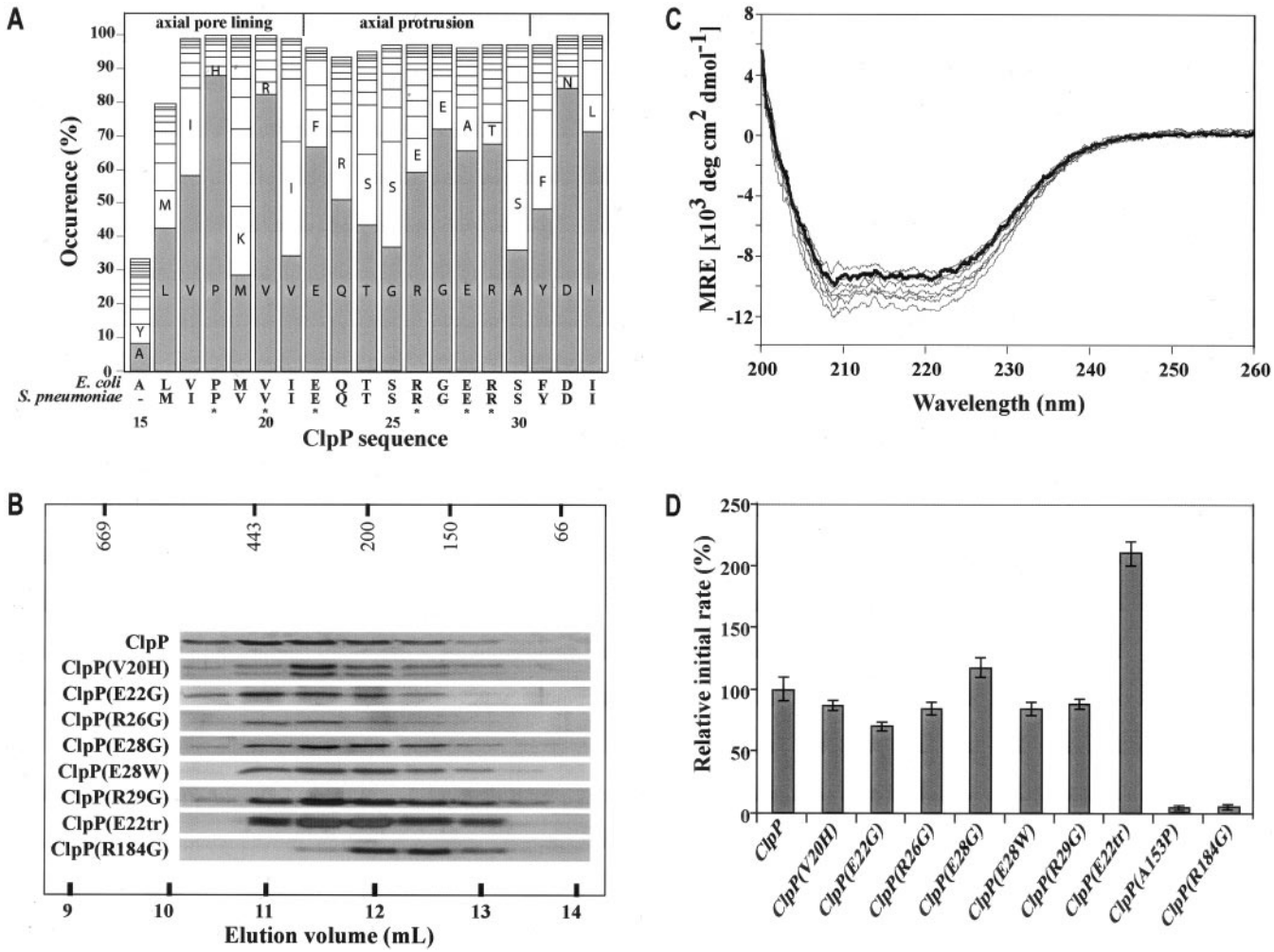

FIG. 6. **ClpP N-terminal mutants are active as peptidases.** *A*, 108 ClpP sequences from bacteria, plant, and mammalian sources were aligned using ClustalW. The most conserved residues according to the Blosum62 matrix are *shaded* in *gray*. Residue numbering is according to the sequence provided by SwissProt (57) for *Ec*ClpP protein (gaps are not included). *Bars* less than 100% are caused by the absence of a residue at the corresponding position in some sequences. Residues at the N terminus of *Ec*ClpP mutated in this study are indicated by an *asterisk*. *B*, the oligomeric state of wild type ClpP and of different mutants in the handle region was analyzed by size exclusion chromatography on a Superdex 200 HR 10/30 column calibrated with buffer A at 4 °C. Fractions were collected at 0.5-ml intervals, and protein fractions were displayed on SDS-polyacrylamide gels and silver stained. The positions of the molecular mass standards, in kDa, are given along the *upper x* axis. The elution profile of ClpP(R184G), which forms a single ring, is shown as a control (*bottom panel*). *C*, far-UV CD spectra, at 22 °C, of wild type ClpP (*dark line*) and the different mutants listed in *B* (*thin lines*) equilibrated in buffer B. The CD signal is expressed as the mean residue ellipticity (*MRE*). *D*, the relative initial rates for the cleavage of Suc-LY-AMC at 37 °C by wild type ClpP and the different listed mutants are shown as a *bar plot* with wild type ClpP set at 100%. *Error bars* indicate the standard deviations calculated from at least three repeats.

observations (Fig. 8*D*) (38). ClpX and wild type ClpP incubated together in the presence of nonhydrolyzable ATP analog, ATPγS, exhibited a significantly increased light scattering intensity compared with ClpX or ClpP alone. This increase in scattering implies the formation of particles significantly larger than either contributing oligomer, an observation consistent with the formation of a complex. Performing the analogous experiment with ClpP(E22tr) did not result in an increased light scattering in the presence of ClpX (Fig. 8*D*). Similarly, the incubation of ClpA with wild type ClpP in the presence of ATPγS resulted in an increased light scattering, whereas no such increase was observed when incubating ClpA and ClpP(E22tr) with ATPγS (Fig. 8*D*). It should be noted that in the presence of ATPγS, ClpA alone showed significant light scattering intensity, whereas ClpX did not, probably because ClpA is about twice the size of ClpX.

The data of Figs. 7 and 8 strongly suggest that the N-terminal axial loops in ClpP are directly involved in the binding between the protease and its ATPases. Hence, in addition to the IGF loop in ClpX or the IGL loop in ClpA (25), the N-terminal loop in ClpP defines another molecular determinant for the interaction between the protease and its ATPases (Fig. 9).

DISCUSSION

Two novel features of ClpP have been revealed by our structural and biochemical experiments. The first feature relates to the plasticity of the handle region and its implications on ring-ring interactions in the ClpP tetradecamer. The second feature relates to the N-terminal axial loops (Fig. 9). We believe that these features provide additional insights into the mechanisms of substrate degradation and release by ClpXP/ClpAP complexes.

Implications of the Alternative Ring-Ring Contacts Observed in SpClpP(A153P)—The *Sp*ClpP(A153P) structure together with the experimental data indicate that the handle region can tolerate partial unfolding and still mediate sufficient ring-ring interactions for ClpP to form a tetradecamer. Truncations in this region do not disrupt the double ring arrangement and do not cause any significant overall conformational change in the

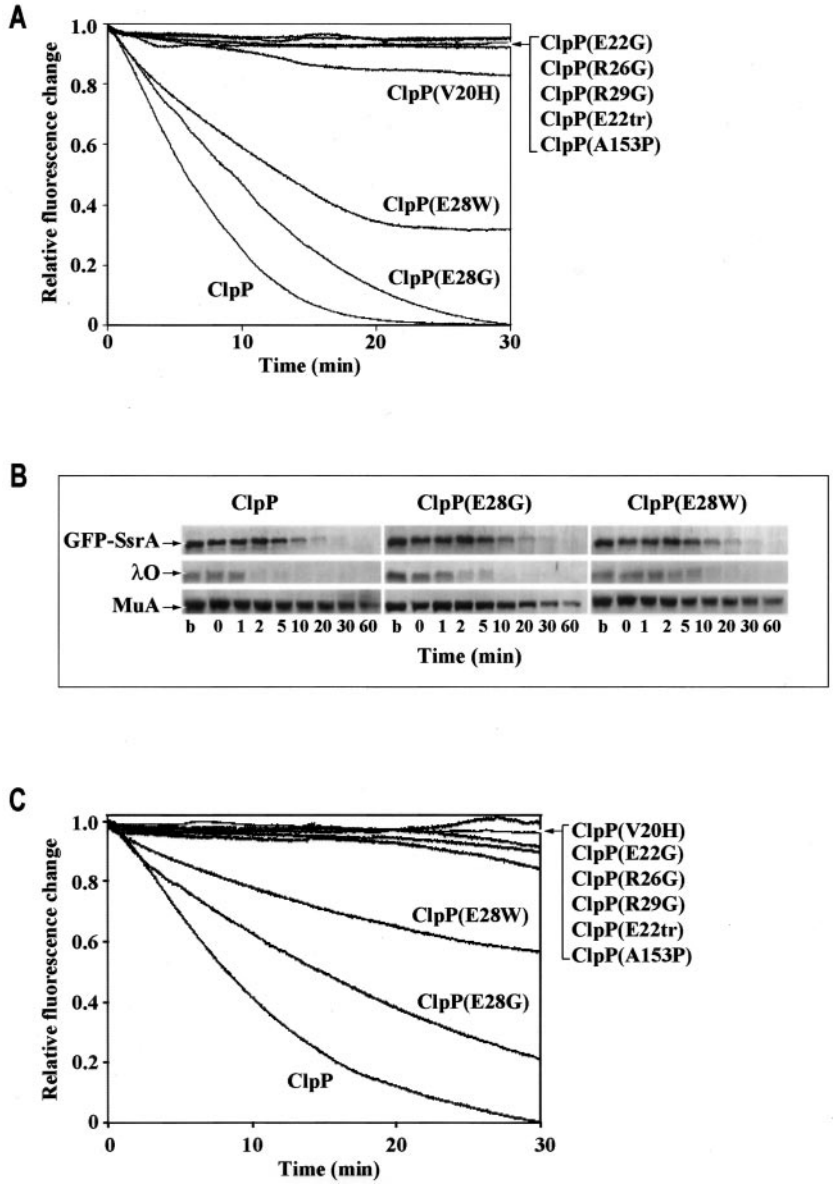

FIG. 7. **Mutations in the N-terminal loop of ClpP affect the degradation of model substrates by ClpXP and ClpAP.** *A*, degradation of GFP-SsrA, monitored by fluorescence at 37 °C, in the presence of ClpX and different ClpP mutants. *B*, the degradation of GFP-SsrA, λO, or MuA in the presence of ClpX and ClpP, ClpP(E28G), or ClpP(E28W) was monitored at 37 °C by separating the proteins on SDS-polyacrylamide gels that were then Coomassie stained. All other N-terminal ClpP mutants cannot degrade these model substrates in the presence of ClpX. In these experiments, ClpX was the last component added. *b* indicates before the addition of ClpX. *C*, degradation of GFP-SsrA, monitored by fluorescence at 37 °C, in the presence of ClpA and different ClpP mutants.

protein as judged by gel filtration, circular dichroism, and ultracentrifugation (Fig. 2). However, charge balance or hydrogen bonding seems to be important as, for example, substitution of the highly conserved Arg^{184} with a neutral glycine residue causes the formation of single ring ClpP under physiological conditions (see Fig. 2*A*).

The solved x-ray structure of *Sp*ClpP(A153P) provides further information on the plasticity of the handle region. The structure shows a novel organization of the ClpP oligomer. In the *Ec*ClpP structure, the two rings are held together by intercalation of their respective handle domains, whereas in the *Sp*ClpP(A153P) structure, the handle domains are mostly unstructured, and the rings interact along a roughly flat surface, leaving several small openings. The interaction through the ring base rather than through the protruding handle domains results in an oligomer that is noticeably shorter in the axial direction with a correspondingly smaller luminal cavity. This structure demonstrates a second mode of ring-ring interaction in ClpP tetradecamer. This could represent an early stage in the assembly of the ClpP oligomer, where two heptameric ClpP rings associate without the handle domains being properly intercalated.

In the observed structure of *Sp*ClpP(A153P), a single Ala → Pro mutation in helix E results in the unfolding of 14 residues including two turns of an α-helix and a β-strand and the loss of numerous interring and intraring interactions. Proline residues are typically considered as helix breakers (42, 43). Calorimetric measurements indicate that a proline residue can destabilize a helix on the order of 1–2 kcal/mol (42, 44). However, studies on T4 lysozyme showed that insertion of proline residues into an existing helix can in many cases result in an active and well structured protein (42). Furthermore, there are many examples of proline residues present within an α-helical structure in a protein; these prolines are generally accommodated through a slight kink in the helix (45). Therefore, the extreme disruption of the handle region caused by the A153P mutation (Figs. 3, *B* and *C*, and 4*B*) would seem to indicate that the handle domain could be intrinsically marginally stable; this might be necessary for the proper assembly or function of ClpP.

Release of degraded protein products from the proteolytic chamber is not fully understood. It has been assumed that degraded substrates exit the ClpP proteolytic channel from an axial pore opposite to the entry pore (21, 27, 46). However, substrate proteins have been observed to bind $(ClpX_6)_2ClpP_{14}$ and $(ClpA_6)_2ClpP_{14}$ complexes from both axial ends, albeit with their denaturation and translocation favored from one end only

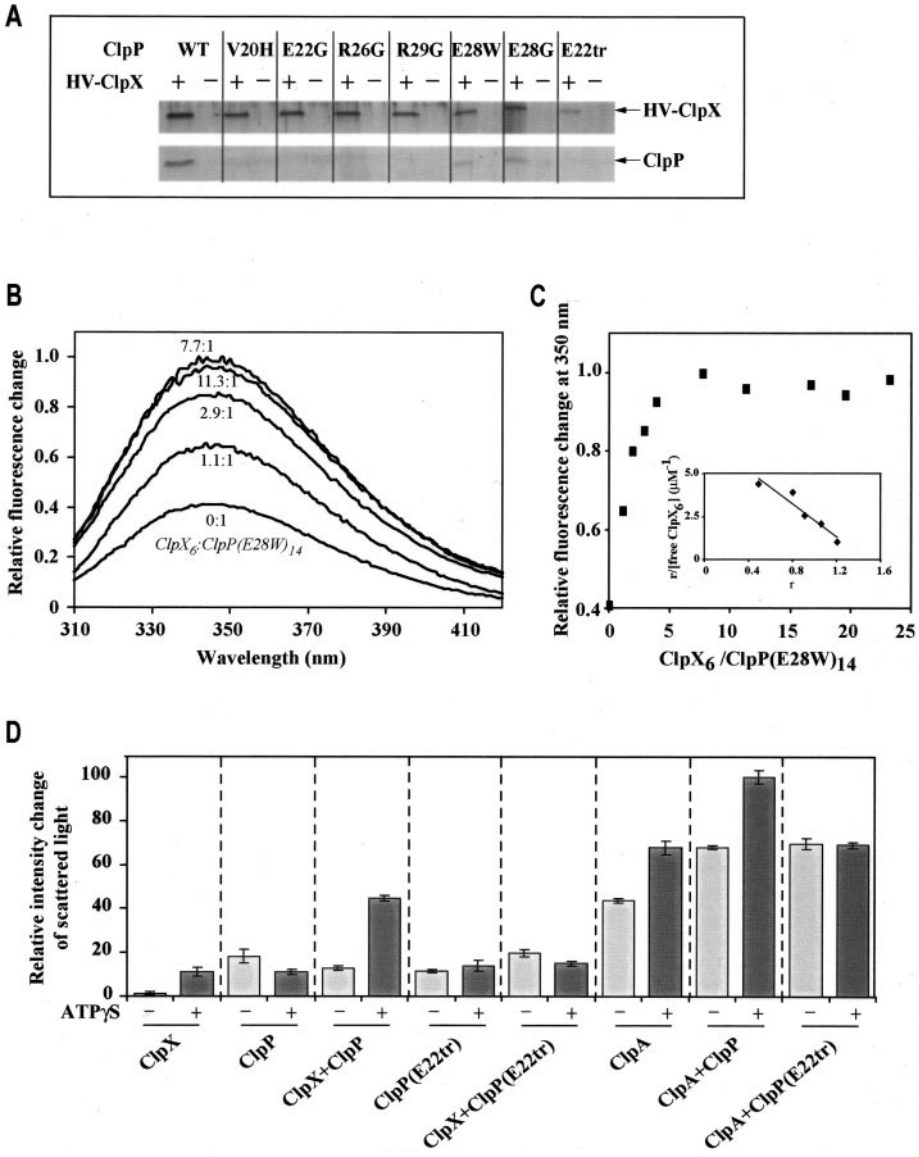

FIG. 8. **Binding between ClpP and ClpX/ClpA is mediated by the N-terminal loops in the protease.** *A*, 1.8 μM untagged wild type ClpP or different N-terminal mutants were incubated with 1 μM HV-ClpX in the presence of 2 mM AMP-PMP for 10 min at 30 °C. Subsequently, Ni^{2+}-NTA resin was added to the mixture, and bound proteins were washed, eluted, separated on SDS-polyacrylamide gels, and silver stained. Only wild type ClpP, ClpP(E28W), and ClpP(E28G) bound to ClpX. *B*, 2.1 μM ClpP(E28W) was incubated at 37 °C with increasing concentrations of ClpX in the presence of 1 mM ATP. Emission scans were obtained after each addition of ClpX using an excitation wavelength of 295 nm. The ratios given indicate the relative molar concentration of $ClpX_6$ to $ClpP(E28W)_{14}$. *C*, a saturation curve for the binding between ClpX and ClpP(E28W) was obtained from fluorescence emission scans like those shown in *B*. The *inset* is an example of a Scatchard plot using the data from the saturation curve for the binding between a ClpX hexamer and ClpP tetradecamer assuming, for simplicity, n identical and independent weak binding sites, giving K_d = 210 nM and n = 1.5 (see "Materials and Methods"). *D*, the interaction between ClpX/ClpA and ClpP or ClpP(E22tr) in the presence of ATPγS was monitored by fluorescence light scattering. An increase in the intensity of scattered light indicates complex formation. *Error bars* represent the S.D. values from four separate experiments.

(24, 28, 38, 47). This simultaneous occlusion at both ends would appear to make the axial pores inefficient exit routes for the release of degraded polypeptides from the ClpP proteolytic chamber. We propose that the plasticity of the strand-turn-helix motif in the handle region, as part of the interface between two heptameric ClpP rings, may hint toward this region being a potential exit site for degraded substrates. However, it should be emphasized that the solved structure of *Sp*ClpP(A153P) is unlikely to represent a configuration of the protein necessary for the catalytic cycle of ClpP because the simultaneous unfolding of all 14 handle domains is unlikely to occur through thermal fluctuations on time scales pertinent to ClpP function. Nevertheless, the *Sp*ClpP(A153P) structure may suggest that residues in the handle region can become unstructured without affecting the rest of the ClpP oligomeric structure. This would make plausible a model in which the strand-turn-helix motif of pairs of handle domains from opposite monomers can temporarily unfold or reorient to create equatorial windows for the exit of degraded peptides. Experiments are currently under way to study this further.

The Structure of the ClpP N-terminal Axial Loops and Their Role in Chaperone Binding—In the *Sp*ClpP(A153P) crystal structure, residues 16–30 at the N-terminal end of the protein form an axial loop, which includes a 9-residue stretch that reaches above the apical surface of the ring (Figs. 3 and 5). This structural feature of the N terminus of *Sp*ClpP(A153P) differs from that published for *Ec*ClpP. To determine whether this difference represents a true structural disparity between the *E. coli* and *S. pneumoniae* proteins or is a result of misinterpretation of the density maps, we used the deposited structure (1TYF) and structure factors (1TYFSF) for *Ec*ClpP to calculate σA-weighted $2F_o - F_c$ and $F_o - F_c$ maps. As Wang *et al.* (21) indicate, the electron density in this region is unclear and difficult to interpret; however, clear negative $F_o - F_c$ difference densities were found associated with the Ser^{30}-Phe^{31} peptide bond and with the side chains of Arg^{26} and Arg^{29} for all 14 monomers. In addition, weak but appreciable density is also visible for residues N-terminal to Phe^{31} in some monomers consistent with at least some kind of extended loop structure. Furthermore, there are several anomalous structural features in this region of the published structure of *Ec*ClpP such as Glu^{28} being completely buried in a hydrophobic pocket, and 14 guanidinium groups contributed by Arg^{26} and Arg^{29} placed in close spatial proximity. Therefore, we believe that there is insufficient information in this region of the electron density map of *Ec*ClpP to claim that the structure of the N-terminal loop in the *E. coli* protein is necessarily different from that in the *S. pneumoniae* protein. Because of the weak electron den-

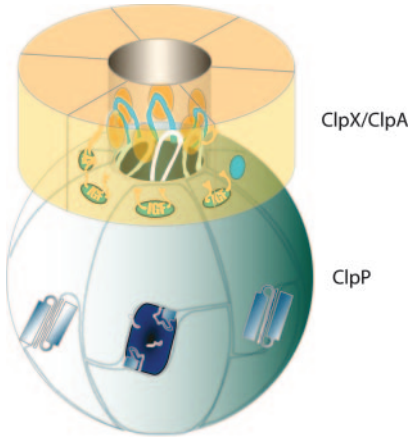

FIG. 9. **Schematic representation of the interaction between ClpP and ClpX/ClpA.** The previously known ClpX IGF loops (or IGL loops in ClpA), which are proposed to bind a site on the ClpP apical surface (25) (*cyan ellipsoids*), are shown as *orange* extensions of the ClpX molecule. As demonstrated by our data, a second critical interaction is mediated by the ClpP N-terminal axial loops, shown as *cyan* to *white* arches, which bind to ClpX (sites indicated by *orange ellipsoids*). Because ClpP has heptameric symmetry whereas ClpX has hexameric symmetry, both the ClpP N-terminal loops and the ClpX IGF loops will adopt different conformations in each monomer to reach their respective binding sites. Also, at any given time, at least one ClpP N-terminal loop is not binding to any ClpX binding site (the *white loop* in the foreground), and at least one IGF binding site on ClpP is unoccupied (*empty cyan ellipse* on the *right*). The possibility that the handle regions of ClpP might become transiently unstructured to form equatorial side windows that allow peptide egress is also illustrated.

sity, the N terminus is probably traced improperly in the published *Ec*ClpP structure, and the loop structures observed in *Sp*ClpP(A153P) (Fig. 5*D*) better approximate reality. However, even in the *Sp*ClpP(A153P) structure this region of the protein is relatively mobile, with residues 25–30 exhibiting average B factors of 58.1 Å^2 compared with an average of 39.9 Å^2 for the rest of the protein; this is a considerable improvement on what is seen in *Ec*ClpP (84 Å^2 and 31 Å^2, respectively). Intriguingly, as in the case of *E. coli* and *S. pneumoniae* ClpPs, the N terminus of the solved structure of another cylindrical bacterial protease, the *Thermoplasma acidophilum* proteasome, is also unstructured (48), indicating a conservation of the flexibility of this region.

In comparing the conformations of the seven monomers in the asymmetric unit of *Sp*ClpP(A153P), it is readily apparent that they diverge quite radically in the N-terminal loop region, not only above the apical surface, but even within the pore itself (Fig. 5*D*). The loop is anchored at the N-terminal end by 6 consecutive hydrophobic residues (Met^{16}, Ile^{17}, Pro^{18}, Val^{19}, Val^{20}, and Ile^{21}) that line the pore and interact with the head domain. For most monomers, the side chains of residues Pro^{18} and Val^{20} are situated in a shallow hydrophobic groove formed by Ile^{33} and Arg^{46} from the same monomer and Ser^{35}, Leu^{38}, Gln^{60}, and Phe^{63} from the neighboring monomer. The side chains of Met^{16} and Ile^{17} point toward the surface of the head domain, whereas the side chains of Val^{19} and Ile^{21} point directly into the axial pore. One possible suggestion is that because the hydrophobic pockets are shallow and relatively nonspecific in nature, the 6 hydrophobic residues might be able to slide relatively freely along this groove giving this region the increased mobility that seems to be an intrinsic property of all ClpP structures. It is possible that rather than forming a passive surface over which polypeptides are translocated, the N-terminal residues in the axial pores of ClpP can adjust dynamically to the entering polypeptide chain to accommodate large and/or awkwardly shaped substrates that would present problems to a more rigid structure. This is in agreement with the results of Burton *et al.* (49) who found that disulfide cross-linked dimers of Arc repressor are efficiently degraded by ClpP even if only one molecule is labeled with an SsrA tag. An axial pore that permits two to three polypeptide chains to be threaded through simultaneously would require an effective diameter on the order of 16–24 Å (49) consistent with the observed pore size in *Sp*ClpP(A153P), about 17 Å.

The high degree of sequence conservation observed for these loops (Fig. 6*A*) suggests that they have an important functional role in ClpP. First, the observation that the ClpP(E22tr) mutant degrades the fluorogenic model peptide substrate Suc-LY-AMC at twice the rate of that exhibited by the wild type protein may indicate that the loops, in the absence of the ATPases, slow down the entrance of small peptides into the ClpP proteolytic lumen or maybe their release. In the *Sp*ClpP(A153P) structure, a subset of the loops, above the apical surface of the pore, partly occlude the pore. This is in general agreement with what has been observed with the core particle of the yeast proteasome (50, 51). In the solved structure of yeast 20 S proteasome, the N termini of the outer α-ring subunits are well defined and project into the axial pores to fill them completely (52). As a result, the particle is autoinhibited by the N-terminal tails that prevent substrate entry into the proteolytic chamber. Deletion of the N-terminal tails results in an enhancement in the peptidase activity of the proteasome toward different fluorogenic peptides.

Perhaps the most important property of the N-terminal loops in ClpP is that they are directly involved in mediating the interaction between the protease and the ATPases. This was demonstrated by the inability of several N-terminal point mutants and an N-terminal truncation of ClpP to degrade model protein substrates that require coupling of the protease to ClpX or ClpA (Fig. 7). All of these mutants were still able to degrade a model dipeptide (Fig. 6*D*). Direct binding between ClpP and the ATPases was demonstrated by pull-down experiments of ClpP using tagged ClpX mutants, fluorescence-based measurements of ClpP(E28W) binding to ClpX, and light scattering experiments that showed that the ClpP(E22tr) variant could not form a complex with ClpX or ClpA (Fig. 8). The experimental data convincingly support the idea that the N-terminal residues of ClpP are essential for, and are directly involved in, the binding between the protease and its ATPase partners. We anticipate that these loops might form more ordered structures upon binding ClpX or ClpA, resulting in an axial pore that is more open above the apical surface than that observed for the *Sp*ClpP(A153P) structure. This possibility is supported by the observation that the degradation of some small peptides is enhanced in the presence of ClpX or ClpA (27, 53). In the case of the 20 S proteasome, it has been observed by x-ray crystallography (54) that the binding of the 11 S regulators to the core protease induces a conformational change causing the N terminus of the α-subunits to adopt a conformation that opens the axial pores.

The details of the interaction between the loops in ClpP and the ATPases have not yet been characterized. In *Sp*ClpP(A153P), Glu^{22}, Arg^{26}, Glu^{28}, and Arg^{29} protrude above the apical surface and are solvent-exposed, and a possible role for a subset of these residues (Glu^{22}, Arg^{26}, and Arg^{29}) in ClpX or ClpA binding has been demonstrated (Figs. 7 and 8). This implies that the interactions between ClpP and its ATPases mediated by the loops are likely largely polar in nature. This is consistent with the observation that, in the *Ec*ClpX hexamer model based on the solved AAA$^+$ domain of *Helicobacter pylori* ClpX (55), the electrostatic potential of the surface of the ATPase facing the protease is highly negatively charged, with the exception of the IGF loops. On the other hand, ClpP with

the V20H point mutation is unable to bind ClpX or ClpA. Val^{20} lies in a shallow, hydrophobic groove formed by residues of the head domain lining the axial pore. The inability of the V20H mutation to bind the chaperones might indicate that tethering of the axial loop in the pore is critical for proper ClpX/ClpA interaction. More complex scenarios, including the possibility that the residues lining the axial pore may somehow rearrange to contact ClpX directly, also cannot be excluded.

Recently, Kang *et al.* (30) solved the structure of human mitochondrial ClpP. They were able to trace the first 7 N-terminal residues of the protease within the lumen. However, unlike our structure of *Sp*ClpP(A153P), they did not observe assignable density for the rest of the residues in the N-terminal loop; nevertheless, they proposed that those residues form a turn outside the core protease. They provided a reinterpretation of the *Ec*ClpP structure similar to that discussed above. Based on biochemical data, the authors proposed that the N-terminal loops of human mitochondrial ClpP might not be important for binding to the ATPases; however, most of the N-terminal mutants they constructed of the human protease were found to be inactive in degrading even small peptides. This was also true for all of the constructed N-terminal truncations. This is a rather perplexing result that contradicts our own observations. It is difficult at this stage to reconcile the results of Kang *et al.* (30) with our own observations, which might point to a major difference between the human mitochondrial and bacterial versions of the ClpP protease.

In summary, the N-terminal loops in bacterial ClpP, in addition to the IGF loop in ClpX or the IGL loop in ClpA (25), define another molecular determinant for the interaction between the protease and its ATPases (Fig. 9). The use of such extended loops to mediate interactions in a hetero-oligomeric complex is rather unusual because protein-protein interactions are more typically mediated by extended interfaces between preordered globular domains (56). The dual use of long flexible loops in this system would seem to serve a specific function to bridge the symmetry mismatch between the hexameric ATPase and the heptameric protease. The flexibility of the axial loops in ClpP and the IGF/IGL loops in ClpX/ClpA might allow the two proteins to maintain their interaction while the two oligomers undergo conformational changes during their functional cycle.

Acknowledgments—We thank Megan Domagala and Bryan Beattie for molecular biology work, Merry-Lynne McDonald for purifying the protein, Simon Houston for crystallizing the protein, and Molly Schmid and Vivek Sharma for helpful discussions.

REFERENCES

1. Gottesman, S., and Maurizi, M. R. (1992) *Microbiol. Rev.* **56,** 592–621
2. Gottesman, S. (1996) *Annu. Rev. Genet.* **30,** 465–506
3. Gottesman, S. (1998) *Proc. Natl. Acad. Sci. U. S. A.* **95,** 2731–2732
4. Katayama, Y., Gottesman, S., Pumphrey, J., Rudikoff, S., Clark, W. P., and Maurizi, M. R. (1988) *J. Biol. Chem.* **263,** 15226–15236
5. Schirmer, E. C., Glover, J. R., Singer, M. A., and Lindquist, S. (1996) *Trends Biochem. Sci.* **21,** 289–296
6. Glover, J. R., and Tkach, J. M. (2001) *Biochem. Cell Biol.* **79,** 557–568
7. Maurizi, M. R., and Xia, D. (2004) *Structure* (*Lond.*) **12,** 175–183
8. Suzuki, C. K., Rep, M., van Dijl, J. M., Suda, K., Grivell, L. A., and Schatz, G. (1997) *Trends Biochem. Sci.* **22,** 118–123
9. Gottesman, S., Wickner, S., and Maurizi, M. R. (1997) *Genes Dev.* **11,** 815–823
10. Feng, H. P., and Gierasch, L. M. (1998) *Curr. Biol.* **8,** R464–R467
11. Dougan, D. A., Mogk, A., Zeth, K., Turgay, K., and Bukau, B. (2002) *FEBS Lett.* **529,** 6–10
12. Gottesman, S., Maurizi, M. R., and Wickner, S. (1997) *Cell* **91,** 435–438
13. Frees, D., and Ingmer, H. (1999) *Mol. Microbiol.* **31,** 79–87
14. Thomsen, L. E., Olsen, J. E., Foster, J. W., and Ingmer, H. (2002) *Microbiology* **148,** 2727–2733
15. Weichart, D., Querfurth, N., Dreger, M., and Hengge-Aronis, R. (2003) *J. Bacteriol.* **185,** 115–125
16. Frees, D., Qazi, S. N., Hill, P. J., and Ingmer, H. (2003) *Mol. Microbiol.* **48,** 1565–1578
17. Kessel, M., Maurizi, M. R., Kim, B., Kocsis, E., Trus, B. L., Singh, S. K., and Steven, A. C. (1995) *J. Mol. Biol.* **250,** 587–594
18. Lupas, A., Flanagan, J. M., Tamura, T., and Baumeister, W. (1997) *Trends Biochem. Sci.* **22,** 399–404
19. Corydon, T. J., Bross, P., Holst, H. U., Neve, S., Kristiansen, K., Gregersen, N., and Bolund, L. (1998) *Biochem. J.* **331,** 309–316
20. Zwickl, P., Baumeister, W., and Steven, A. (2000) *Curr. Opin. Struct. Biol.* **10,** 242–250
21. Wang, J., Hartling, J. A., and Flanagan, J. M. (1997) *Cell* **91,** 447–456
22. Ortega, J., Singh, S. K., Ishikawa, T., Maurizi, M. R., and Steven, A. C. (2000) *Mol. Cell* **6,** 1515–1521
23. Ishikawa, T., Beuron, F., Kessel, M., Wickner, S., Maurizi, M. R., and Steven, A. C. (2001) *Proc. Natl. Acad. Sci. U. S. A.* **98,** 4328–4333
24. Ortega, J., Lee, H. S., Maurizi, M. R., and Steven, A. C. (2002) *EMBO J.* **21,** 4938–4949
25. Kim, Y. I., Levchenko, I., Fraczkowska, K., Woodruff, R. V., Sauer, R. T., and Baker, T. A. (2001) *Nat. Struct. Biol.* **8,** 230–233
26. Joshi, S. A., Hersch, G. L., Baker, T. A., and Sauer, R. T. (2004) *Nat. Struct. Mol. Biol.* **11,** 404–411
27. Thompson, M. W., Singh, S. K., and Maurizi, M. R. (1994) *J. Biol. Chem.* **269,** 18209–18215
28. Maurizi, M. R., Singh, S. K., Thompson, M. W., Kessel, M., and Ginsburg, A. (1998) *Biochemistry* **37,** 7778–7786
29. Peltier, J. B., Ripoll, D. R., Friso, G., Rudella, A., Cai, Y., Ytterberg, J., Giacomelli, L., Pillardy, J., and van Wijk, K. J. (2004) *J. Biol. Chem.* **279,** 4768–4781
30. Kang, S. G., Maurizi, M. R., Thompson, M., Mueser, T., and Ahvazi, B. (2004) *J. Struct. Biol.* **148,** 338–352
31. Seol, J. H., Yoo, S. J., Kang, M. S., Ha, D. B., and Chung, C. H. (1995) *FEBS Lett.* **377,** 41–43
32. Wojtyra, U. A., Thibault, G., Tuite, A., and Houry, W. A. (2003) *J. Biol. Chem.* **278,** 48981–48990
33. Lo, J. H., Baker, T. A., and Sauer, R. T. (2001) *Protein Sci.* **10,** 551–559
34. Otwinowski, Z., and Minor, W. (1997) *Methods Enzymol.* **276,** 307–326
35. Brunger, A. T., Adams, P. D., Clore, G. M., DeLano, W. L., Gros, P., Grosse-Kunstleve, R. W., Jiang, J. S., Kuszewski, J., Nilges, M., Pannu, N. S., Read, R. J., Rice, L. M., Simonson, T., and Warren, G. L. (1998) *Acta Crystallogr. Sect. D Biol. Crystallogr.* **54,** 905–921
36. Roussel, A., and Cambillan, C. (1989) *Silicon Graphics Geometry Partner Directory*, pp. 77–78, Silicon Graphics, Mountain View, CA
37. Woo, K. M., Chung, W. J., Ha, D. B., Goldberg, A. L., and Chung, C. H. (1989) *J. Biol. Chem.* **264,** 2088–2091
38. Singh, S. K., Guo, F., and Maurizi, M. R. (1999) *Biochemistry* **38,** 14906–14915
39. Jones, J. M., Welty, D. J., and Nakai, H. (1998) *J. Biol. Chem.* **273,** 459–465
40. Kaplan, W., and Littlejohn, T. G. (2001) *Brief Bioinform.* **2,** 195–197
41. Freifelder, D. M. (1982) in *Physical Biochemistry: Applications to Biochemistry and Molecular Biology* (Freifelder, D., ed), 2nd Ed., pp. 537–547, W. H. Freeman, San Francisco
42. Sauer, U. H., San, D. P., and Matthews, B. W. (1992) *J. Biol. Chem.* **267,** 2393–2399
43. Gray, T. M., Arnoys, E. J., Blankespoor, S., Born, T., Jagar, R., Everman, R., Plowman, D., Stair, A., and Zhang, D. (1996) *Protein Sci.* **5,** 742–751
44. Chakrabarti, A., Srivastava, S., Swaminathan, C. P., Surolia, A., and Varadarajan, R. (1999) *Protein Sci.* **8,** 2455–2459
45. Gunasekaran, K., Nagarajaram, H. A., Ramakrishnan, C., and Balaram, P. (1998) *J. Mol. Biol.* **275,** 917–932
46. Kim, Y. I., Burton, R. E., Burton, B. M., Sauer, R. T., and Baker, T. A. (2000) *Mol. Cell* **5,** 639–648
47. Ortega, J., Lee, H. S., Maurizi, M. R., and Steven, A. C. (2004) *J. Struct. Biol.* **146,** 217–226
48. Lowe, J., Stock, D., Jap, B., Zwickl, P., Baumeister, W., and Huber, R. (1995) *Science* **268,** 533–539
49. Burton, R. E., Siddiqui, S. M., Kim, Y. I., Baker, T. A., and Sauer, R. T. (2001) *EMBO J.* **20,** 3092–3100
50. Groll, M., Bajorek, M., Kohler, A., Moroder, L., Rubin, D. M., Huber, R., Glickman, M. H., and Finley, D. (2000) *Nat. Struct. Biol.* **7,** 1062–1067
51. Kohler, A., Bajorek, M., Groll, M., Moroder, L., Rubin, D. M., Huber, R., Glickman, M. H., and Finley, D. (2001) *Biochimie* (*Paris*) **83,** 325–332
52. Groll, M., Ditzel, L., Lowe, J., Stock, D., Bochtler, M., Bartunik, H. D., and Huber, R. (1997) *Nature* **386,** 463–471
53. Grimaud, R., Kessel, M., Beuron, F., Steven, A. C., and Maurizi, M. R. (1998) *J. Biol. Chem.* **273,** 12476–12481
54. Whitby, F. G., Masters, E. I., Kramer, L., Knowlton, J. R., Yao, Y., Wang, C. C., and Hill, C. P. (2000) *Nature* **408,** 115–120
55. Kim, D. Y., and Kim, K. K. (2003) *J. Biol. Chem.* **278,** 50664–50670
56. Goodsell, D. S., and Olson, A. J. (2000) *Annu. Rev. Biophys. Biomol. Struct.* **29,** 105–153
57. Boeckmann, B., Bairoch, A., Apweiler, R., Blatter, M. C., Estreicher, A., Gasteiger, E., Martin, M. J., Michoud, K., O'Donovan, C., Phan, I., Pilbout, S., and Schneider, M. (2003) *Nucleic Acids Res.* **31,** 365–370